Environmental Science & Technology

Article

pubs.acs.org/est

Performance and Mechanisms of Ultrafiltration Membrane Fouling Mitigation by Coupling Coagulation and Applied Electric Field in a Novel Electrocoagulation Membrane Reactor

Jingqiu Sun,[†,‡] Chengzhi Hu,[*,†,§] Tiezheng Tong,[§] Kai Zhao,[†] Jiuhui Qu,[†] Huijuan Liu,[†] and Menachem Elimelech[§]

[†]Key Laboratory of Drinking Water Science and Technology, Research Center for Eco-Environmental Sciences, Chinese Academy of Sciences, Beijing 100085, China

[‡]University of Chinese Academy of Science, Beijing 100049, China

[§]Department of Chemical and Environmental Engineering, Yale University, New Haven, Connecticut 06520-8286, United States

Supporting Information

ABSTRACT: A novel electrocoagulation membrane reactor (ECMR) was developed, in which ultrafiltration (UF) membrane modules are placed between electrodes to improve effluent water quality and reduce membrane fouling. Experiments with feedwater containing clays (kaolinite) and natural organic matter (humic acid) revealed that the combined effect of coagulation and electric field mitigated membrane fouling in the ECMR, resulting in higher water flux than the conventional combination of electrocoagulation and UF in separate units (EC-UF). Higher current densities and weakly acidic pH in the EMCR favored faster generation of large flocs and effectively reduced membrane pore blocking. The hydraulic resistance of the formed cake layers on the membrane surface in ECMR was reduced due to an increase in cake layer porosity and polarity, induced by both coagulation and the applied electric field. The formation of a polarized cake layer was controlled by the applied current density and voltage, with cake layers formed under higher electric field strengths showing higher porosity and hydrophilicity. Compared to EC-UF, ECMR has a smaller footprint and could achieve significant energy savings due to improved fouling resistance and a more compact reactor design.

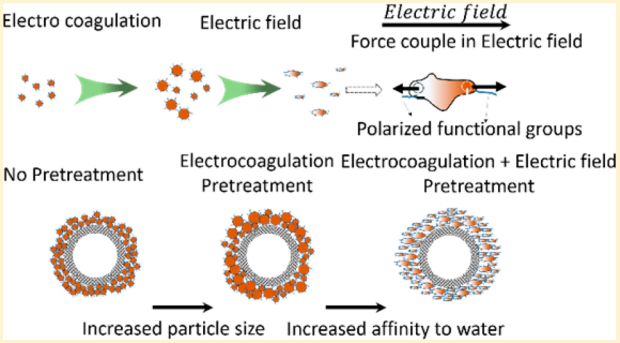

INTRODUCTION

Pressure-driven membrane filtration technologies are widely used in water treatment.[1] Ultrafiltration (UF) in particular is commonly employed in drinking water treatment because it removes multiple contaminants in one step and is economically feasible.[2,3] However, UF is inherently constrained by membrane fouling, with dissolved organic substances (e.g., humic acid and proteins) acting as major foulants.[4−6] Membrane fouling compromises the performance and lifetime of UF membranes, increasing the cost and energy demand of UF systems. Therefore, effective strategies for fouling mitigation are highly desirable to improve the efficiency and applicability of UF systems.[7]

Electrocoagulation (EC) is an attractive process in water treatment, and its performance and mechanisms have been widely investigated.[8] Since EC could effectively remove particles and humic acid from raw water, applying EC as a pretreatment step is one of the promising solutions to control UF membrane fouling.[9−14] The properties of flocs generated by EC have a significant influence on the structure of membrane cake layers and the extent of membrane fouling.[9,11] For example, it has been reported that the steady-state normalized specific water flux increased from 51% for microfiltration to 72% for electrocoagulation-microfiltration.[15] If the porosity and structure of the formed cake layer can be effectively controlled in the EC process, a highly porous protective layer could be formed to further alleviate membrane fouling.

Applied electric field has also been considered as an efficient method to reduce membrane fouling.[16−18] It has been demonstrated that deposition of charged foulants, such as humic acid and inorganic particles, was prevented by electrostatic repulsion induced by an electric field.[19,20] In this case, charged foulants migrate away from the membrane surface by electrostatic force.[21,22] It was further suggested that the dipole moment of foulants can also influence membrane fouling.[23] Although electric field can alter the dipole moment of organic foulants, its effect on cake layer structure has not been investigated. Furthermore, previous studies typically combined EC with membrane filtration as separate units,[8,24,25] in which

Received: March 5, 2017
Revised: June 19, 2017
Accepted: July 11, 2017
Published: July 11, 2017

DOI: 10.1021/acs.est.7b01189
Environ. Sci. Technol. 2017, 51, 8544−8551

membranes were located outside of the electric field zone. We hypothesize that when EC and UF are integrated in one unit, membrane fouling would be mitigated by the combined effect of both coagulation and electric field, leading to further improvement of membrane fouling control.

In this study, we designed an integrated electrocoagulation membrane reactor (ECMR), with membrane modules placed between a pair of electrodes. We evaluated the efficiency of ECMR in mitigating membrane fouling, and analyzed the effect of electrochemical parameters on the ECMR performance. To better understand the antifouling mechanisms of ECMR, we focused on the evolution of particle size and cake layer polarity in ECMR, which are influenced by coagulation and electric field, respectively. Our study is the first to propose the concept of ECMR and systematically delineate its design and working principles.

MATERIALS AND METHODS

Chemicals and Synthetic Feed Water. A stock solution of humic acid (Sigma-Aldrich) was prepared in deionized water (DI, Millipore Milli-Q) after filtration through a 0.45 μm mixed cellulose ester membrane. The molecular weight of humic acid was mainly distributed around ~270 kDa and ~10 kDa (Supporting Information (SI) Figure S1).The prepared stock solution had a dissolved organic carbon (DOC) concentration of 777 ± 20 mg/L and was stored at 4 °C until use. Sodium chloride (50 mM) was added in the synthetic feedwater as the background electrolyte, and sodium bicarbonate (0.5 mM) was used to provide a buffer capacity. DOC of the synthetic feedwater was adjusted to 5 mg/L and clay (kaolinite) concentration to 50 mg/L. Sodium hydroxide and hydrochloric acid were used to adjust the solution pH for experiments investigating the effect of pH on ECMR performance. Sodium chloride, sodium bicarbonate, sodium hydroxide, and hydrochloric acid were received at analytical pure grade; kaolinite was at chemical pure grade with particle size ranging from ~400 to ~1200 nm (SI Figure S2). The ATR-FTIR spectra of humic acid and kaolinite are presented in SI Figure S3. All reagents were purchased from Sinopharm Chemical Regent Co., Ltd., China.

ECMR System and Membrane Fouling Experiments. Figure 1 describes the design of the ECMR system and membrane modules. The UF membrane module was placed between two plate electrodes, so that both the EC process and applied electric field could work in concert to mitigate membrane fouling in one unit. When the membrane module was placed outside the electrodes, the process was considered as an EC-UF system instead of ECMR. Unlike other systems that combined (electro) coagulation with ultrafiltration or microfiltration,[10,15,26] EC-UF was performed in one single reactor in our study. The effective volume of the reactor was 735 mL (14 × 5 × 10.5 cm). As shown in Figure 1b, hollow fiber membranes (PVDF, Tianjin MOTIMO Membrane Technology Co., Ltd., China) were used in the UF system. A membrane module composed of ten fibers with a length of 3 cm was employed to provide an effective membrane area of 24 cm^2. A small tube was placed on top of the membrane module for permeate collection. According to the manufacturer, the membrane average molecular weight cutoff was 100 kDa, which is corresponding to an average pore size of ~30 nm.

In each experiment, 1.4 L of synthetic feedwater was recycled by two peristaltic pumps (36 mL/min) in order to generate cross-flow and keep a constant water level in the ECMR system

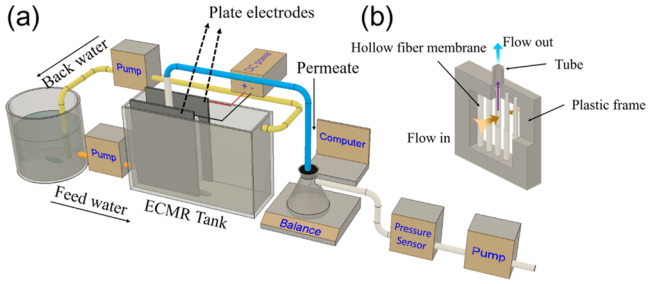

Figure 1. Schemes for (a) the design of ECMR system: 1.4 L of synthetic feedwater was recycled by two peristaltic pumps (36 mL/min) in order to generate cross-flow and keep a constant water level in the ECMR system. The membrane module was placed between two aluminum electrodes parallel to the water flow, with the distance between the two electrodes fixed at 2.5 cm. A pressure sensor was employed to monitor the transmembrane pressure, which was maintained at 30 kPa by a peristaltic pump. Permeate water was generated via peristaltic pump from UF membrane module and weighted by a digital balance, which connected to a computer. (b) Hollow fiber membrane module (one-eighth was cut off in order to exhibit the inside structure of the membrane module). Water passed through membranes from the fiber outside (brown arrow), flowed inside the membranes (purple arrow) and was collected by a small tube on top of the membrane module (blue arrow).

(Figure 1 and SI Figure S4). The membrane module was placed between two aluminum electrodes parallel to the water flow, with the distance between the two electrodes fixed at 2.5 cm. The feedwater was well mixed by a magnetic stirrer at 300 rpm. A digital balance (ME2002E, Mettler Toledo, Switzerland) connected to a personal computer was used to record the mass of permeate during system operation. A pressure sensor was employed to monitor the transmembrane pressure, which was maintained at 30 kPa by a peristaltic pump. The initial water flux of each membrane module was 96.25 $L{\cdot}m^{-1}{\cdot}h^{-1}$. Unless otherwise specified, pH was adjusted to 7.0 and the current density was 10 A/m^2. When investigating the effects of electric field strength on membrane fouling, different electrolyte concentrations were used to keep the current density constant. The electrolyte concentration (measured as conductivity) exhibited little effect on water flux in our experiments (SI Figure S5).

Analytical Methods. UV absorbance at 254 nm (UV_{254}) was measured by an ultraviolet−visible spectrophotometer (U-3010, Hitachi High Technologies Co., Japan) as an indicator of humic acid concentration. Dissolved organic carbon (DOC, after filtration through 0.45 μm mixed cellulose ester membranes) was determined with a total organic carbon (TOC) analyzer (TOC-VCPH, Shimadzu, Japan).

In order to investigate cake layer properties, fouled membrane fibers were cut from the membrane modules and dried at room temperature for 24 h. In the preparation of cross-section samples of membranes, the hollow fiber membranes were frozen in liquid nitrogen, and then cut instantly to preserve the cake layer attached to the membrane surface. The pristine and fouled membrane samples were platinum-coated by a sputter and observed under a scanning electron microscope (SEM, JSM7401F, JEDL, Japan). Attenuated total reflectance Fourier transform infrared (ATR-FTIR) spectra were collected by a Fourier Transform Infrared Spectrometer (Nicolet 8700, Thermo Fisher Scientific). Furthermore, the hydrophilicity of the fouled membranes formed under different electric fields was measured by a dynamic contact angle

DOI: 10.1021/acs.est.7b01189
Environ. Sci. Technol. 2017, 51, 8544−8551

tensiometer (Data Physics DCAT, LPD Lab Services Ltd., UK). Floc size as a function of time was directly monitored by a laser particle size analyzer (Mastersizer 2000, Malvern, UK).[27] The flocs were monitored by pumping water through the optical unit of the laser particle size analyzer and back into the reactor by a peristaltic pump on the return tube (5 mm internal diameter). Particle size was recorded every 20 s during the experiments by a computer.

RESULTS AND DISCUSSION

Performance of ECMR. The removal rate of humic acid (as measured by UV_{254}) and membrane water flux were measured to evaluate the performance of ECMR compared to EC-UF, EC, and UF (Figure 2). As shown in Figure 2a, the removal rate

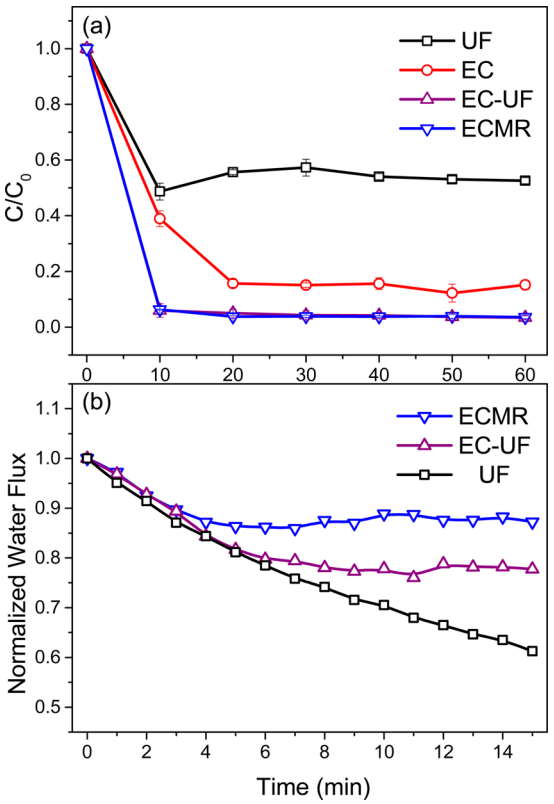

Figure 2. (a) Removal rate of humic acid (as measured by UV_{254}) by UF, EC, EC-UF, and ECMR. Removal rates were obtained from three independent fouling experiments. (b) Final relative water flux (J/J_0) of ECMR and EC-UF at 10 A/m^2 and UF alone. Feed water was composed of sodium chloride (50 mM), sodium bicarbonate (0.5 mM), humic acid (5 mg/L DOC), and kaolinite (50 mg/L). Initial solution pH was 7.0 and temperature was kept at 25 °C.

of humic acid by ECMR attained 93.7 ± 0.2% within 10 min and maintained the same level afterward. This removal rate was comparable to that of EC-UF (94.0 ± 2.5%), but significantly higher than those of EC (61.1 ± 2.9%) and UF (51.3 ± 3.0%). For UF, size exclusion is the main mechanism for humic acid removal. The low removal efficiency of humic acid by UF indicates that humic acid macromolecules smaller than the membrane pore size were able to pass through the UF membrane. Although higher removal efficiency (~80%) could be achieved by EC than UF, longer time was needed for floc sedimentation. The ECMR and EC-UF processes combined the advantages of the EC and UF processes to achieve a much higher removal efficiency of humic acid within a short time.

As shown in Figure 2b, water flux decline of ECMR caused by membrane fouling was less than that observed with EC-UF and UF. The flux decline curves for ECMR and EC-UF exhibited two stages that corresponded to different fouling mechanisms, consistent with the pore blockage−cake filtration model developed by Ho and Zydney.[28] This model accounts for a smooth transition of fouling mechanism from pore blockage to cake formation during filtration, and has been successfully used in investigating humic acid fouling in microfiltration.[29] Our observation indicates that initial fouling was due to deposition of humic acid aggregates on the membrane surface blocking membrane pores, followed by formation of a cake layer on the regions of membrane that had been covered by the foulant aggregates.

The water flux for UF alone decreased continuously within 15 min, suggesting that pore blocking played a primary role. In contrast, a rapid flux decline was only observed in the beginning period (i.e., the first 4−7 min) for ECMR and EC-UF. After this initial period, the water flux was maintained at a relatively steady level, indicating that a cake layer had been formed on the membrane surface. This two-stage mode of flux decline was consistent with the results reported in other studies (SI Table S1).[30−32] The final relative water flux, J/J_0, of the ECMR (87.2%) was higher than that of EC-UF (77.8%). Therefore, ECMR achieved comparable humic acid rejection but provided a higher water flux than EC-UF. This finding indicates that coagulation and electric field likely influence the structure and physicochemical properties of the formed cake layer, which will be discussed in more detail in the following subsections.

Key Operational Parameters Governing EMCR Fouling Behavior. Water flux decline by pore blockage mechanism depends on foulant size.[33] Severe membrane fouling can be caused by pore blocking when the particle size is comparable to the membrane pore size. As the EC process proceeds, particle size increases in the coagulation process.[34,35] Furthermore, current density and pH could control aluminum coagulant dosage and hydrolysis rate, respectively, thereby leading to different sizes of generated flocs.[36]

As shown in Figure 3a, an increase of current density promoted fouling resistance in ECMR. Under a current density of 2 A/m^2, the water flux of ECMR decreased to 70.5% of the initial value and kept steady afterward. When the current density increased to 10 A/m^2 and 20 A/m^2, the water fluxes were maintained at 83.1% and 97.3% of the original flux, respectively. Furthermore, the applied current density influenced the growth of particles formed in ECMR. As shown in Figure 3b, particles kept stable at first and then started to grow in size rapidly at 2, 4, and 11 min under current densities of 20 A/m^2, 10 A/m^2, and 2 A/m^2, respectively. Notably, this critical time for particle growth roughly matched the inflection point of the flux decline curve when water flux became stable.

The electric field strengths varied with the different current densities applied in ECMR, thereby creating two variables (electric field strength and current density) that potentially influenced membrane fouling. This dependence may interfere with the interpretation of the observed flux decline curves under different current densities (Figure 3). Therefore, the effect of current density on water flux was investigated in EC-UF (i.e., UF membrane outside the reactor and under no electric field) to exclude the concomitant influence of electric field. As shown in SI Figure S6, the trend of flux decline under

DOI: 10.1021/acs.est.7b01189
Environ. Sci. Technol. 2017, 51, 8544−8551

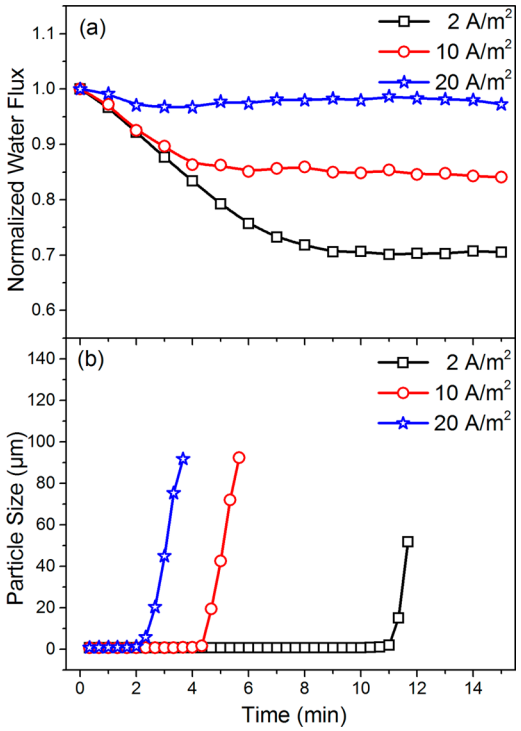

Figure 3. (a) Normalized water flux decline curves at different current densities in ECMR; (b) particle size evolution with time at different current densities at initial pH 7. Feed solution composition is described in the caption of Figure 2.

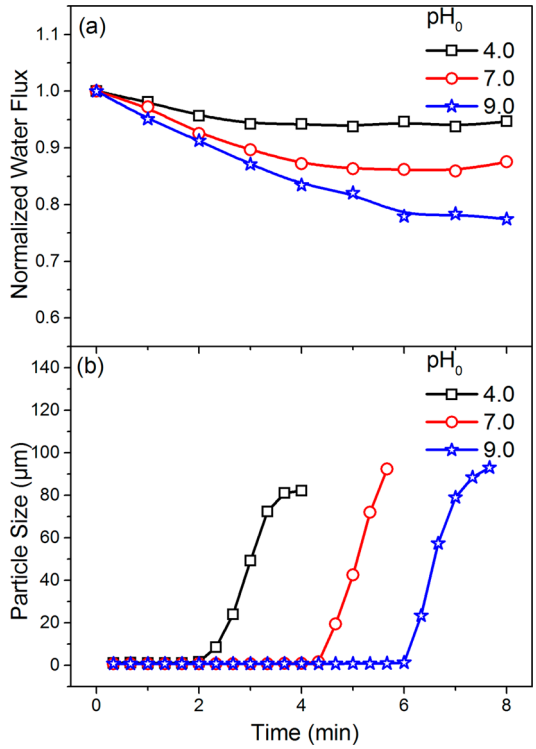

Figure 4. (a) Normalized water flux decline curves under different initial solution pH; (b) particle size evolution with time under different initial solution pH at 10 A/m^2. Feed solution composition is described in the caption of Figure 2.

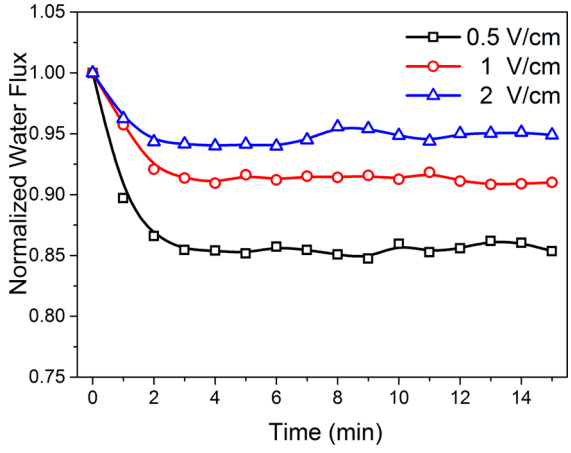

Figure 5. Normalized water flux decline curves under different initial electric field strengths. The corresponding initial electric conductivities were 500, 1000, and 2000 μS/cm for 2.00 V/cm, 1.00 V/cm, and 0.50 V/cm, respectively; current density was 10 A/m^2 at pH 7.0. Feed solution composition is described in the caption of Figure 2.

various current densities in EC-UF was consistent with that in ECMR. This observation suggests that higher current densities produced more aluminum coagulant species per unit time, thus enhancing aggregation of foulants (humic acid and kaolinite) and reducing membrane fouling.

Solution pH also influenced EMCR performance because pH governs the coagulation mechanisms and the growth of particles by metal salt coagulants.[35,37,38] According to our previous work,[38] lower solution pH resulted in a more rapid growth of flocs with a more porous structure, which might contribute to the mitigation of membrane fouling. As shown in Figure 4a, J/J_0 reached a steady state of 94.7% at pH 4.0, whereas it decreased to 87.6% and 77.4% at pH 7.0 and 9.0, respectively. Figure 4b shows that the particle size kept small initially and then started to grow rapidly at 2, 4, and 6 min for pH at 4.0, 7.0, and 9.0, respectively. Consistent with the phenomenon observed in Figure 3, the time when particle size started to increase roughly matched the inflection point of the flux decline curves for every pH, which underscores the importance of particle size in reducing membrane fouling in ECMR.

Our results demonstrate that current density and solution pH are two critical parameters for membrane fouling control in ECMR. Hence, proper control of these operational parameters could be used to optimize membrane resistance to pore blocking.

Cake Layer Properties under Applied Electric Field. Water flux decline curves under various initial electric field strengths are presented in Figure 5. The current density was kept constant, whereas the electric field strength was varied by altering the electric conductivity of the feed solutions. Electrolyte concentration (measured as conductivity) exhibited negligible effect on membrane fouling and humic acid removal in our experiments (SI Figure S5 and S7). Feed solutions with lower conductivities resulted in stronger electric field strengths. Results show that the final normalized water flux (J/J_0) was positively correlated to the initial strength of the electric field. Specifically, J/J_0 values were 85.4%, 91.0%, and 94.9% under electric field strengths of 0.5 V/cm, 1 V/cm, and 2 V/cm, respectively. Polarization effects induced by the electric field likely played an important role in membrane fouling, especially during the process of cake layer formation, as also recently observed by Fan et al.[20] To further explore this observation, we analyzed the morphology and hydrophilicity of the fouled

DOI: 10.1021/acs.est.7b01189
Environ. Sci. Technol. 2017, 51, 8544−8551

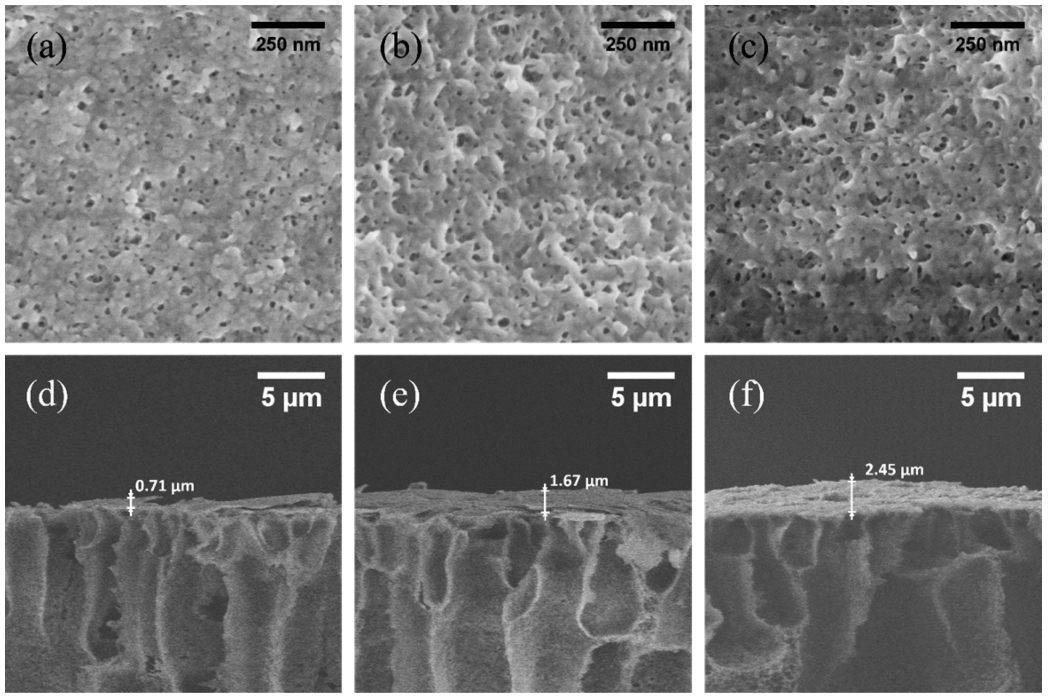

Figure 6. Scanning electron microscopy (SEM) images of fouled hollow fiber membrane surface under electric fields of (a) 0.5 V/cm, (b) 1 V/cm, and (c) 2 V/cm and cross sections under electric fields of (d) 0.5 V/cm, (e) 1 V/cm, and (f) 2 V/cm, respectively. The corresponding initial conductivities were 500, 1000, and 2000 μS/cm, for 2 V/cm, 1 V/cm, and 0.5 V/cm, respectively; current density was 10 A/m^2 at pH 7.0 and experiment time was 30 min. Feed solution composition is described in the caption of Figure 2.

membranes in order to understand the alteration of cake layer properties under different electric fields.

The surface morphologies of the fouled membranes subjected to different electric field strengths were observed by SEM (Figure 6a-c). The cake layers formed under different electric field showed similar compositions (SI Figure S8). But when the strength of electric field increased, the cake layer showed a more irregular and rougher surface with enhanced porosity. The observed average pore sizes of the cake/fouling layers were 7.9, 12.6, and 12.8 nm under electric field strengths of 0.5 V/cm, 1 V/cm, and 2 V/cm, respectively (SI Figure S9). Also, the thickness of cake layers was larger at higher electric field strengths (Figure 6d–f).

As the electric field increases, the structure of the formed cake layers is increasingly influenced by orientation polarization.[39] Negatively charged functional groups would orient toward the anode and positively charged groups would orient toward the cathode, which results in more functional groups oriented parallel to the direction of electric field. In addition, the surface charge of the foulants could be enhanced by displacement polarization.[40] The foulant molecules would be stretched along the direction of electric field, and the end functional groups on foulants could concentrate more charges. Therefore, the interaction between foulants is strengthened in the direction parallel to electric field. In contrast, this interaction was weakened perpendicular to electric field, resulting in an increased pore size of cake layers. According to this mechanism, charged foulants under higher electric field strengths were more prone to be connected to attach to the membrane surface, contributing to an increase of cake layer thickness.

Figure 7 indicates that cake layers formed under higher electric field strengths were more hydrophilic than those formed at a lower electric field strength. As the electric field

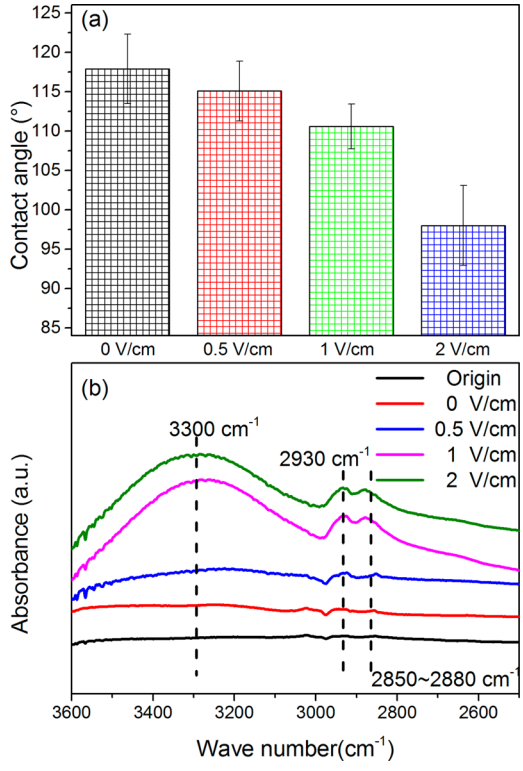

Figure 7. (a) Contact angle and (b) attenuated total reflectance Fourier transform infrared spectroscopy (ATR-FTIR) spectra of fouled membranes at different initial electric fields. The corresponding initial conductivities were 500, 500, 1000, and 2000 μS/cm, for 0 V/cm, 2 V/cm, 1 V/cm, and 0.5 V/cm, respectively; the current density was 10 A/m^2 at pH 7.0. Contact angle measurements were repeated three times.

DOI: 10.1021/acs.est.7b01189
Environ. Sci. Technol. 2017, 51, 8544–8551

strength increased from 0.5 V/cm to 2 V/cm, the water contact angle of the fouled membrane surface decreased from 114.7 ± 5.3° to 99.4 ± 6.3° (Figure 7a). It has been reported that a more hydrophilic cake layer resulted in a greater membrane fouling resistance in UF.[41] Furthermore, ATR-FTIR was used to characterize the surface functionality of the fouled membranes. The peaks at 2850−2880 cm^{-1}, 2930 cm^{-1} (aliphatic C−H stretching), and 3300 cm^{-1} (O−H stretching vibration), which are characteristic for humic substances,[36,42−44] showed higher signals as the electric fields increased from 0 V/cm to 2 V/cm (Figure 7b). This result indicates an increase of humic acid amount in the cake layers, which was in agreement with the thicker cake layer observed at higher electric field strengths. Many functional groups of humic acid, such as carboxyl, hydroxyl and amine groups, are known to be influenced by electric field,[39] in particular hydroxyl and amide groups that have higher electric dipole moments and are more readily polarized. In addition, charge distribution with foulant (humic acid) molecules was induced by the applied electric field, resulting in more charges being concentrated at both ends of the molecules along electric field direction. These polarized functional groups rendered humic acid more inclined to attach to the membrane surface at higher electric fields due to the stronger electrostatic force. As a result, cake layers with higher polarity were formed, exhibiting high affinity to water molecules and subsequently improving water permeability. An illustration of the proposed mechanism for the impact of electric field on fouling is summarized in Figure 8.

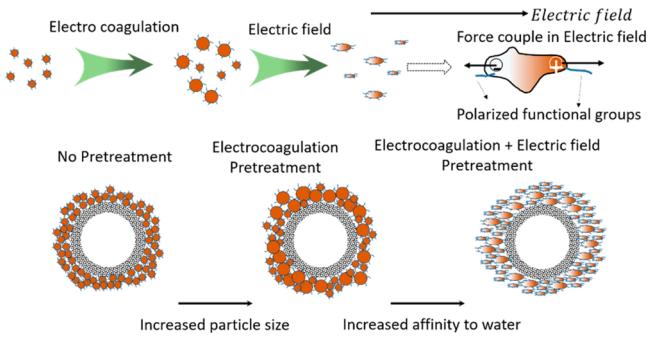

Figure 8. Schematic description of the proposed mechanisms for membrane fouling mitigation in ECMR.

ECMR Fouling Mitigation Mechanisms and Implications for System Operation and Design. Particle size, which performed as a key factor in reducing membrane fouling in ECMR, was controlled by the current density and solution pH. Particles with sizes larger than the membrane pore size reduced membrane pore blocking and facilitated the formation of a cake layer that served as a protective layer. Meanwhile, a loose and hydrophilic cake layer was formed in ECMR, due to oriented polarization of foulants under the electric field. Charged foulants on the membrane surface were aligned in accordance with the direction of the applied electric field. The increased cake layer polarity induced by both coagulation and electric field further improved the affinity of the membranes to water. Therefore, the combined effect of coagulation and electric field in ECMR improved the fouling resistance of UF the membrane and resulted in a higher water flux.

ECMR not only improves removal efficiency of organic matter but also greatly mitigates membrane fouling. ECMR performs better at high current densities and under weakly acidic pH conditions. It is also feasible to further minimize membrane pore blocking by starting the membrane filtration process after the floc size becomes larger than the membrane pore size. Furthermore, increasing the applied voltage can result in a more hydrophilic cake layer. The above operation conditions favor effective mitigation of membrane fouling in practice.

Water production per unit volume of reactor can be increased with the design of multiple electrodes and membrane modules in the ECMR. The energy consumption per unit water production for ECMR at 2 A/m^2 was comparable to that of EC-UF. When applying current densities of 10 A/m^2 and 20 A/m^2, ECMR reduces energy consumption by 6.4% and 1.3%, respectively, compared to EC-UF (SI Table S2 and eq S8). Therefore, energy savings could be achieved by changing the water treatment system configuration from EC-UF to ECMR. In addition, the land use of ECMR will be reduced due to a more compact reactor design.

■ ASSOCIATED CONTENT

Supporting Information

The Supporting Information is available free of charge on the ACS Publications website at DOI: 10.1021/acs.est.7b01189.

Molecular weight distribution of humic acid (Figure S1); particle size distribution of kaolinite (Figure S2); ATR-FTIR spectra of humic acid and kaolinite (Figure S3); supplementary scheme for the design of ECMR (Figure S4); normalized water flux decline curves at different electric conductivity (Figure S5); calculation of particle size for light scattering measurements; fitted parameters for pore blocking resistance-limited model (Table S1); normalized water flux decline curves at different current densities in EC-UF (Figure S6); influence of ionic strength on EC (Figure S7); energy dispersion spectrum analysis (Figure S8); pore size analysis (Figure S9); parameters for energy consumption calculation (Table S2) (PDF)

■ AUTHOR INFORMATION

Corresponding Author

*Phone: +86-10-62849160; fax: +86-10-62849160; e-mail: czhu@rcees.ac.cn.

ORCID

Chengzhi Hu: 0000-0001-9898-835X
Jiuhui Qu: 0000-0001-9177-093X
Huijuan Liu: 0000-0003-0855-0202
Menachem Elimelech: 0000-0003-4186-1563

Author Contributions

The manuscript was written through contributions of all authors. All authors have given approval to the final version of the manuscript.

Notes

The authors declare no competing financial interest.

■ ACKNOWLEDGMENTS

We are grateful for financial support from the National Natural Science Foundation of China (No. 51678556 and 51438011) and the Major Science and Technology Program for Water Pollution Control and Treatment (2015ZX07402003-3).

DOI: 10.1021/acs.est.7b01189
Environ. Sci. Technol. 2017, 51, 8544−8551

REFERENCES

(1) Shannon, M. A.; Bohn, P. W.; Elimelech, M.; Georgiadis, J. G.; Marinas, B. J.; Mayes, A. M. Science and technology for water purification in the coming decades. *Nature* **2008**, *452* (7185), 301−310.

(2) Van der Bruggen, B.; Everaert, K.; Wilms, D.; Vandecasteele, C. Application of nanofiltration for removal of pesticides, nitrate and hardness from ground water: rejection properties and economic evaluation. *J. Membr. Sci.* **2001**, *193* (2), 239−248.

(3) Zhang, Q.; Vecitis, C. D. Conductive CNT-PVDF membrane for capacitive organic fouling reduction. *J. Membr. Sci.* **2014**, *459*, 143−156.

(4) Saravia, F.; Zwiener, C.; Frimmel, F. H. Interactions between membrane surface, dissolved organic substances and ions in submerged membrane filtration. *Desalination* **2006**, *192* (1−3), 280−287.

(5) Jermann, D.; Pronk, W.; Meylan, S.; Boller, M. Interplay of different NOM fouling mechanisms during ultrafiltration for drinking water production. *Water Res.* **2007**, *41* (8), 1713−1722.

(6) Peiris, R. H.; Halle, C.; Budman, H.; Moresoli, C.; Peldszus, S.; Huck, P. M.; Legge, R. L. Idendifying fouling events in a membrane-based drinking water treatment process using principal component analysis of fluorescence excitation-emission matrices. *Water Res.* **2010**, *44* (1), 185−194.

(7) Chung, C. M.; Tobino, T.; Cho, K.; Yamamoto, K. Alleviation of membrane fouling in a submerged membrane bioreactor with electrochemical oxidation mediated by in-situ free chlorine generation. *Water Res.* **2016**, *96*, 52−61.

(8) Bagga, A.; Chellam, S.; Clifford, D. A. Evaluation of iron chemical coagulation and electrocoagulation pretreatment for surface water microfiltration. *J. Membr. Sci.* **2008**, *309* (1−2), 82−93.

(9) Gamage, N. P.; Chellam, S. Aluminum electrocoagulation pretreatment reduces fouling during surface water microfiltration. *J. Membr. Sci.* **2011**, *379* (1−2), 97−105.

(10) Ben Sasson, M.; Adin, A. Fouling mechanisms and energy appraisal in microfiltration pretreated by aluminum-based electro-flocculation. *J. Membr. Sci.* **2010**, *352* (1−2), 86−94.

(11) Hua, L.-C.; Huang, C.; Su, Y.-C.; Tran-Ngoc-Phu, N.; Chen, P.-C. Effects of electro-coagulation on fouling mitigation and sludge characteristics in a coagulation-assisted membrane bioreactor. *J. Membr. Sci.* **2015**, *495*, 29−36.

(12) Huang, H.; Schwab, K.; Jacangelo, J. G. Pretreatment for Low Pressure Membranes in Water Treatment: A Review. *Environ. Sci. Technol.* **2009**, *43* (9), 3011−3019.

(13) Chellam, S.; Sari, M. A. Aluminum electrocoagulation as pretreatment during microfiltration of surface water containing NOM: A review of fouling, NOM, DBP, and virus control. *J. Hazard. Mater.* **2016**, *304*, 490−501.

(14) Ibeid, S.; Elektorowicz, M.; Oleszkiewicz, J. A. Electro-conditioning of activated sludge in a membrane electro-bioreactor for improved dewatering and reduced membrane fouling. *J. Membr. Sci.* **2015**, *494*, 136−142.

(15) Sari, M. A.; Chellam, S. Surface water nanofiltration incorporating (electro) coagulation-microfiltration pretreatment: Fouling control and membrane characterization. *J. Membr. Sci.* **2013**, *437*, 249−256.

(16) Bani-Melhem, K.; Elektorowicz, M. Development of a Novel Submerged Membrane Electro-Bioreactor (SMEBR): Performance for Fouling Reduction. *Environ. Sci. Technol.* **2010**, *44* (9), 3298−3304.

(17) Liu, L.; Liu, J.; Gao, B.; Yang, F.; Chellam, S. Fouling reductions in a membrane bioreactor using an intermittent electric field and cathodic membrane modified by vapor phase polymerized pyrrole. *J. Membr. Sci.* **2012**, *394*, 202−208.

(18) Ronen, A.; Duan, W.; Wheeldon, I.; Walker, S.; Jassby, D. Microbial Attachment Inhibition through Low-Voltage Electrochemical Reactions on Electrically Conducting Membranes. *Environ. Sci. Technol.* **2015**, *49* (21), 12741−12750.

(19) Chen, J.-P.; Yang, C.-Z.; Zhou, J.-H.; Wang, X.-Y. Study of the influence of the electric field on membrane flux of a new type of membrane bioreactor. *Chem. Eng. J.* **2007**, *128* (2−3), 177−180.

(20) Fan, X.; Zhao, H.; Quan, X.; Liu, Y.; Chen, S. Nanocarbon-based membrane filtration integrated with electric field driving for effective membrane fouling mitigation. *Water Res.* **2016**, *88*, 285−292.

(21) Tsai, Y.-T.; Weng, Y.-H.; Lin, A. Y.-C.; Li, K.-C. Electro-microfiltration treatment of water containing natural organic matter and inorganic particles. *Desalination* **2011**, *267* (2−3), 133−138.

(22) Chen, X.; Deng, H. Removal of humic acids from water by hybrid titanium-based electrocoagulation with ultrafiltration membrane processes. *Desalination* **2012**, *300*, 51−57.

(23) Nghiem, L. D.; Schafer, A. I.; Elimelech, M. Pharmaceutical retention mechanisms by nanofiltration membranes. *Environ. Sci. Technol.* **2005**, *39* (19), 7698−7705.

(24) Zhu, B. T.; Clifford, D. A.; Chellam, S. Comparison of electrocoagulation and chemical coagulation pretreatment for enhanced virus removal using microfiltration membranes. *Water Res.* **2005**, *39* (13), 3098−3108.

(25) Tanneru, C. T.; Rimer, J. D.; Chellam, S. Sweep Flocculation and Adsorption of Viruses on Aluminum Flocs during Electrochemical Treatment Prior to Surface Water Microfiltration. *Environ. Sci. Technol.* **2013**, *47* (9), 4612−4618.

(26) Chen, Y.; Dong, B. Z.; Gao, N. Y.; Fan, J. C. Effect of coagulation pretreatment on fouling of an ultrafiltration membrane. *Desalination* **2007**, *204* (1−3), 181−188.

(27) Yu, W.; Hu, C.; Liu, H.; Qu, J. Effect of dosage strategy on Al-humic flocs growth and re-growth. *Colloids Surf., A* **2012**, *404*, 106−111.

(28) Ho, C. C.; Zydney, A. L. A combined pore blockage and cake filtration model for protein fouling during microfiltration. *J. Colloid Interface Sci.* **2000**, *232* (2), 389−399.

(29) Yuan, W.; Kocic, A.; Zydney, A. L. Analysis of humic acid fouling during microfiltration using a pore blockage-cake filtration model. *J. Membr. Sci.* **2002**, *198* (1), 51−62.

(30) Lee, S.; Cho, J. W.; Elimelech, M. Combined influence of natural organic matter (NOM) and colloidal particles on nanofiltration membrane fouling. *J. Membr. Sci.* **2005**, *262* (1−2), 27−41.

(31) Xiao, F.; Xiao, P.; Zhang, W. J.; Wang, D. S. Identification of key factors affecting the organic fouling on low-pressure ultrafiltration membranes. *J. Membr. Sci.* **2013**, *447*, 144−152.

(32) Yuan, W.; Zydney, A. L. Humic acid fouling during microfiltration. *J. Membr. Sci.* **1999**, *157* (1), 1−12.

(33) Howe, K. J.; Marwah, A.; Chiu, K.-P.; Adham, S. S. Effect of coagulation on the size of MF and UF membrane foulants. *Environ. Sci. Technol.* **2006**, *40* (24), 7908−7913.

(34) Xu, Y.; Chen, T.; Cui, F.; Shi, W. Effect of reused alum-humic-flocs on coagulation performance and floc characteristics formed by aluminum salt coagulants in humic-acid water. *Chem. Eng. J.* **2016**, *287*, 225−232.

(35) Ching, H. W.; Elimelech, M.; Hering, J. G. Dynamics of Coagulation of Clay Particles with Aluminum Sulfate. *J. Environ. Eng.* **1994**, *120* (1), 169−189.

(36) Tremblay, L.; Alaoui, G.; Leger, M. N. Characterization of Aquatic Particles by Direct FTIR Analysis of Filters and Quantification of Elemental and Molecular Compositions. *Environ. Sci. Technol.* **2011**, *45* (22), 9671−9679.

(37) Cao, B.; Gao, B.; Liu, X.; Wang, M.; Yang, Z.; Yue, Q. The impact of pH on floc structure characteristic of polyferric chloride in a low DOC and high alkalinity surface water treatment. *Water Res.* **2011**, *45* (18), 6181−6188.

(38) Hu, C.; Sun, J.; Wang, S.; Liu, R.; Liu, H.; Qu, J. Enhanced efficiency in HA removal by electrocoagulation through optimizing flocs properties: Role of current density and pH. *Sep. Purif. Technol.* **2017**, *175*, 248−254.

(39) de Menezes, V. M.; Mota, R.; Zanella, I.; Fagan, S. B. Pristine and functionalized capped carbon nanotubes under electric fields. *Phys. Status Solidi B* **2014**, *251* (3), 649−654.

DOI: 10.1021/acs.est.7b01189
Environ. Sci. Technol. 2017, 51, 8544−8551

(40) Li, H.; Hu, T.; Zhang, R.; Liu, J.; Hou, W. Preparation of solid-state Z-scheme Bi_2MoO_6/MO (M = Cu, $Co_{3/4}$, or Ni) heterojunctions with internal electric field-improved performance in photocatalysis. *Appl. Catal., B* **2016**, *188*, 313−323.
(41) Peter-Varbanets, M.; Margot, J.; Traber, J.; Pronk, W. Mechanisms of membrane fouling during ultra-low pressure ultra-filtration. *J. Membr. Sci.* **2011**, *377* (1−2), 42−53.
(42) Litvin, V. A.; Minaev, B. F. Spectroscopy study of silver nanoparticles fabrication using synthetic humic substances and their antimicrobial activity. *Spectrochim. Acta, Part A* **2013**, *108*, 115−122.
(43) Hatch, C. D.; Gierlus, K. M.; Zahardis, J.; Schuttlefield, J.; Grassian, V. H. Water uptake of humic and fulvic acid: measurements and modelling using single parameter Kohler theory. *Environ. Chem.* **2009**, *6* (5), 380−388.
(44) Jarusutthirak, C.; Amy, G. Role of soluble microbial products (SMP) in membrane fouling and flux decline. *Environ. Sci. Technol.* **2006**, *40* (3), 969−974.

DOI: 10.1021/acs.est.7b01189
Environ. Sci. Technol. 2017, 51, 8544−8551